Electronic Supplementary Information: Doping $MAPbBr_3$ Hybrid Perovskites with CdSe/CdZnS Quantum Dots: from Emissive Thin Films to Hybrid Single-Photon Sources

Justine Baronnier[†], Julien Houel[†*], Christophe Dujardin[†], Florian Kulzer[†], and Benoît Mahler[†*]

February 22, 2022

Contents

[†] Institut Lumière-Matière, CNRS UMR5306, Université Lyon 1, Université de Lyon, 69622 Villeurbanne CEDEX, France

[*] To whom correspondence should be addressed: julien.houel@univ-lyon1.fr, benoit.mahler@univ-lyon1.fr

1 Gaussian Fits of QD Photoluminescence Spectra

Figure S1 shows the photoluminescence spectra of the samples that are discussed in the main article with Gaussian fits to the QD emission peaks; the results of the fit procedure are summarized in Table S1.

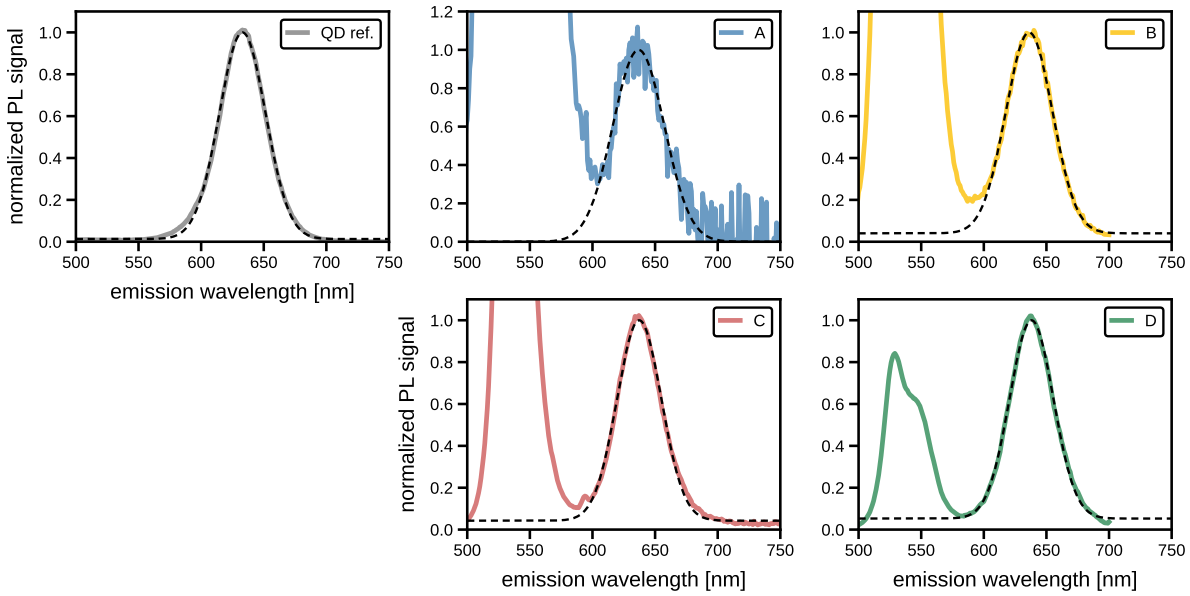

Figure S1: Photoluminescence spectra of a reference sample (bare QDs on a BK7 substrate) and of four QD-in-perovskite hybrid films (samples A – D); the excitation wavelength was 405 nm in all cases. The spectra presented here are the same ones as in Figs. 2 a/b of the main article, now normalized to the height of each QD emission band for convenience. The dashed lines are fits of Gaussian peaks to the data, using the full spectrum for the QD reference and the region above 600 nm for the four hybrid films, respectively.

Table S1: Center wavelengths and full widths at half maximum (FWHM) of the Gaussian fit curves shown in Fig. S1; the uncertainties of the fit parameters are based on the Levenberg-Marquardt covariance matrices.

sample	center [nm]	FWHM [nm]
QD reference	633.0 ± 0.1	43.7 ± 0.2
sample A	636.8 ± 0.7	48.3 ± 2.2
sample B	636.2 ± 0.1	43.9 ± 0.3
sample C	637.3 ± 0.1	41.8 ± 0.2
sample D	638.1 ± 0.1	41.1 ± 0.3

2 Further Characterization of the QD-Doped Thin Films of $MAPbBr_3$

In this section, we present further data on the crystalline structure of the doped perovskite films as well as on the homogeneity of the distribution of the QDs and their photostability after extended shelf storage under ambient conditions. Figure S2 compares two X-ray diffraction diagrams of $MAPbBr_3$ thin film, one undoped and the other one doped with CdSe/CdZnS QDs at 1 % (nominal). As can be seen, the positions and widths of the X-ray diffraction peaks remained unchanged by the doping procedure, suggesting conservation of the perovskite crystalline structure; only changes in the relative intensity of the peaks were observed and potentially a week and broad new band at $2\theta \approx 48°$.

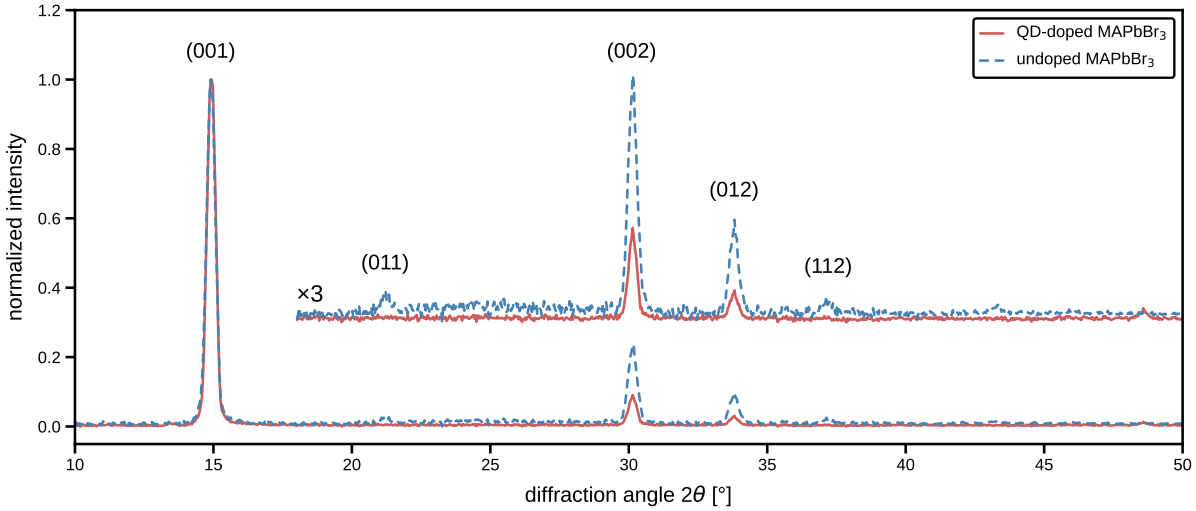

Figure S2: X-ray diffraction diagrams of an undoped $MAPbBr_3$ thin film (dashed line) and a CdSe/CdZnS-doped film (solid line). The region $2\theta \geqslant 18°$ is additionally shown with three-times magnification and a vertical offset of 0.25 added for clarity; diffraction peaks have been labeled with the Miller indices of the corresponding lattice planes.

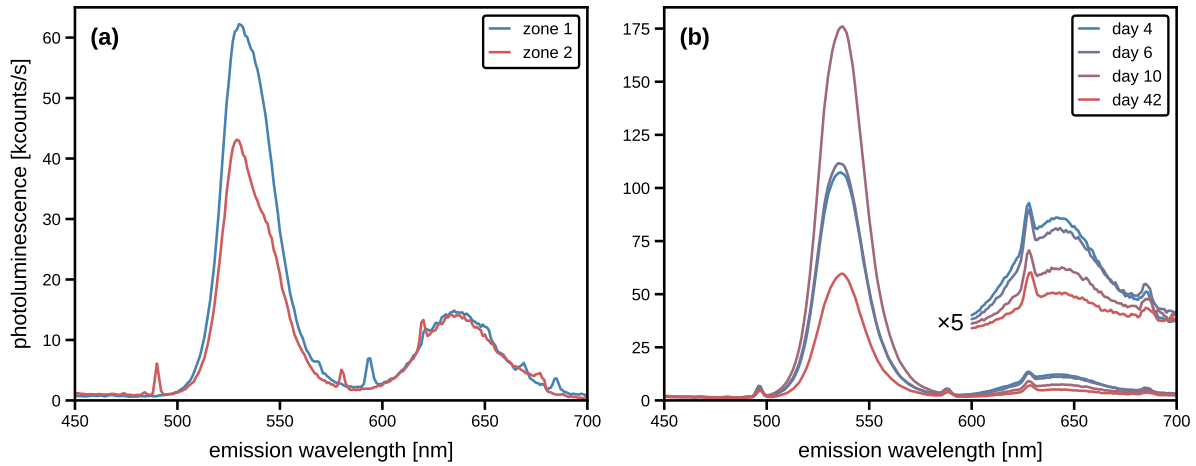

Figure S3: Homogeneity and stability of QD-photoluminescence (PL) spectra. (a) PL spectra of two different macroscopic areas of the same CdSe/CdZnS-doped $MAPbBr_3$ thin film. (b) PL spectra of CdSe/CdZnS QDs in a thin $MAPbBr_3$ film recorded after 4, 6, 10, and 42 days of shelf storage under ambient atmosphere. The spectral region of the QD emission band, $\lambda \geqslant 600\,\mathrm{nm}$, is additionally shown with five-times magnification and a vertical offset of 25 added for clarity; the small-intensity spikes on the spectra are known spectrometer artifacts in thin-film geometry.

Figure S3 a shows two PL spectra recorded under identical excitation conditions on two different regions of the same sample: While the $MAPbBr_3$ emission of the perovskite (centered around 530 nm) exhibits the usual spatial dependency, the emission of the QDs ($\lambda \geqslant 640$ nm) was fairly constant, indicating a high degree of macroscopic homogeneity in the spatial distribution of the QDs over the sample. As can be seen in Fig. S3 b, which documents the evolution of a QD-in-perovskite PL emission spectrum for a sample that was stored under ambient atmosphere for over a month, the QD signal (centered around 640 nm) was roughly constant up to day 6, had dropped by half after 10 days, and then remained fairly stable once again until day 42. We found significant sample-to-sample variation of this photostability, with some films exhibiting an almost complete loss of the QD PL signal after a few days, while others, like the example of Fig. S3 b, retained significant QD emission even after more than one month of shelf storage.

3 Normalization of PLE Spectra

In order to illustrate the normalization procedure of the photoluminescence excitation (PLE) employed in the main article and to motivate our choice of normalization region, we present here the original PLE spectra before normalization. Figure S4 a shows the absorption spectrum of the pure perovskite film, whose absorption is negligible in the normalization region (550 – 600 nm). Figures S4 b, c, d compare the PLE spectrum of sample A, sample B and the QD reference film, respectively, to a PLE spectrum of a solution of the QDs in DMF; the solution spectrum was originally published in Ref. S1 and has been rescaled here to the same average intensity in the normalization region of each respective thin-film spectrum. While the PLE spectrum of the bare QDs on BK7 agrees with the rescaled solution spectrum over the whole spectral range within experimental noise limits, the PLE spectra of samples A and B exhibit a noticeably different behavior even in the normalization region and deviate significantly outside of it, especially at shorter wavelengths. The limits of our normalization region where therefore chosen to both steer clear of the perovskite absorption band below 550 nm and to avoid the more pronounced deviations above 600 nm. Note that the PLE spectrum of sample B is only about two times as intense in the normalization region as the PLE spectrum of sample A, while one would expect a factor of four based on the ratio of the nominal doping percentages; this discrepancy is due to differences in excitation and detection conditions that were necessary to ensure optimal recording of both spectra over the whole wavelength range from 400 to 630 nm.

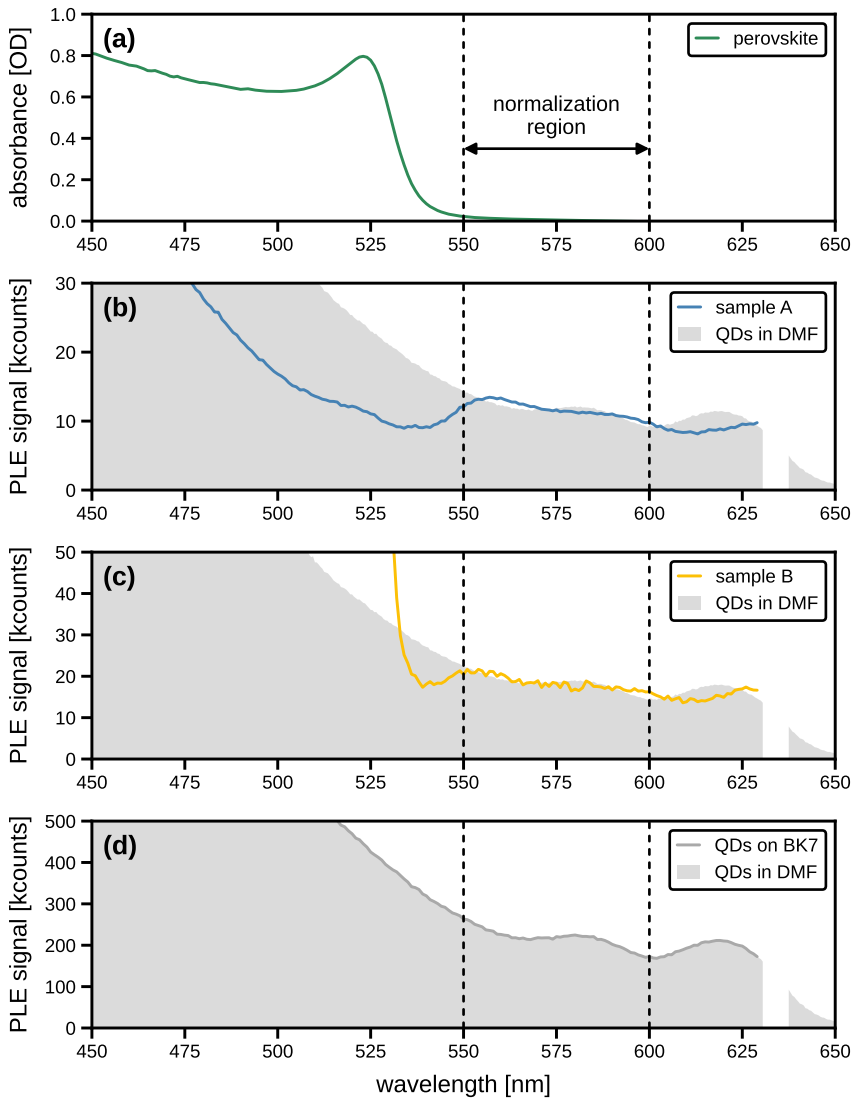

Figure S4: Comparison of the perovskite absorption spectrum with the photoluminescence excitation (PLE) spectra of QD-in-perovskite hybrid films (samples A and B), of bare QDs on a BK7 substrate, and of a solution of QDs in DMF. The spectral region used for normalization of the PLE spectra in Fig. 2 c is indicated by dashed vertical lines. (a) Absorption spectrum of $MAPbBr_3$, same data as in Fig. 1 a. (b) PLE spectrum of sample A compared to a PLE spectrum of QDs in DMF [S1] that has been rescaled to the same average intensity in the normalization region. [The gap in the solution spectrum indicates the masked detection window, which was $\lambda_{\mathrm{det}} = (634 \pm 3)\,\mathrm{nm}$ in this particular case.] (c) PLE spectrum of sample B compared to the rescaled solution spectrum. (d) PLE spectrum of the QD reference film (bare QDs on BK7), again shown with the rescaled solution spectrum.

4 QD Radiative Lifetime as a Function of Perovskite Refractive Index

A comparison between the luminescence antibunching curves of a single QD-in-perovskite hybrid (Fig. 6 c of the main article) and of an individual QD on BK7 [S1] is presented in Fig. S5. We attribute the observed large difference in the exponential rise times τ_{QD} of the QDs in the two environments to the influence of the refractive index on their radiative lifetime, in accordance with an effective-medium model described in earlier publications, in which we showed that CdSe/ZnS QDs act as probes for the local refractive index of their environment within a sphere of sensitivity whose radius ranges from 50 to 100 nm [S2–S4].

Our approach is based on the virtual cavity (VC) model, which can be written as:

$$\gamma_{\mathrm{vac}} = \frac{\gamma_{\mathrm{ref}}}{\bar{n}_{\mathrm{ref}}} \left(\frac{3}{\bar{n}_{\mathrm{ref}}^2 + 2} \right)^2 \qquad \text{and} \tag{S1}$$

$$\gamma_{\mathrm{mat}} = \left(\frac{\bar{n}_{\mathrm{mat}}^2 + 2}{3} \right)^2 \bar{n}_{\mathrm{mat}}\, \gamma_{\mathrm{vac}} \qquad , \tag{S2}$$

where γ_{ref}, γ_{mat} and γ_{vac} are the exciton recombination rates of CdSe/CdZnS QDs spincast on a BK7 coverslip, in the $MAPbBr_3$ matrix and in vacuum, respectively, while $\bar{n}_{\mathrm{ref}}$ and $\bar{n}_{\mathrm{mat}}$ are the effective refractive indices experienced by the QDs in these two types of samples; we calculated these effective indices using the Bruggeman effective-medium approach [S5].

For the reference sample ($n_{\mathrm{BK7}} = 1.52$), we find $\bar{n}_{\mathrm{ref}} = 1.22$, while the effective refractive index for the QD-in-perovskite heterostructure ($n_{\mathrm{MAPbBr_3}} = 2.10$, determined by ellipsometry at 650 nm) is $\bar{n}_{\mathrm{mat}} = 1.84$, if we assume a homogeneous distribution of the QDs in the hybrid film and average over its thickness. Inserting $\bar{n}_{\mathrm{ref}}$ and $\gamma_{\mathrm{ref}} = 0.026\,\mathrm{ns}^{-1}$ (from the measured $\tau_{\mathrm{ref}} = 39$ ns) into the VC model of Eq. (S1), we obtain $\gamma_{\mathrm{vac}} = 0.016\,\mathrm{ns}^{-1}$, which corresponds to an exciton recombination lifetime in vacuum of $\tau_{\mathrm{vac}} = 64$ ns. The value of γ_{vac} thus identified leads to an expected radiative lifetime for the QD-in-perovskite hybrid of $\tau_{\mathrm{hybrid}} = 11$ ns when used in Eq. (S2), which agrees very well with our average experimental value of (12 ± 4) ns. The above estimate of 11 ns was obtained with a assumed radius of influence of $R = 80$ nm, in accordance with our previous results on CdSe-based QDs [S2–S4].

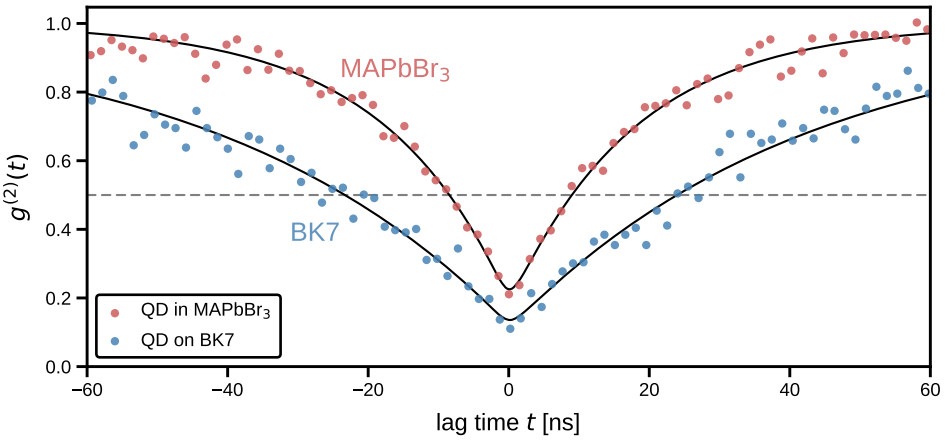

Figure S5: The antibunching measurement performed on a QD-in-perovskite hybrid (Fig. 6 c) compared to the same experiment on another individual QD on BK [S1]. The solid curves represent maximum-likelihood adjustments of the model of Eq. (4) to the data, which yield $\tau_{\mathrm{QD}} = (17.7 \pm 0.4)$ ns and $\tau_{\mathrm{QD}} = (42.3 \pm 4.2)$ ns for the QD in perovskite and the one on BK7, respectively.

5 Blinking Behavior and Median Survival Times of CdSe/CdZnS QDs in $MAPbBr_3$ and on BK7

Figure S6 compares the PL emission blinking of a QD in $MAPbBr_3$ to that of a matrix-free individual QD deposited on BK7. Both QDs had a comparable overall emission intensity and exhibited a bimodal count rate histogram arising from stochastic transitions between a bright "on" state and a dim "off" state. Using the classification algorithm reported earlier [S1], we found an ON time fraction of 95 % for this particular QD-in-perovskite hybrid, compared to 64 % for the bare QD on glass. We furthermore found that the median survival time before photobleaching of the QDs on BK7 was 120 s, while that of the QDs in perovskite was greater than 300 s (the total observation time in these experiments), leading us to conclude that the survival time of single QDs under illumination is increased by at least 150 % due to the insertion in the perovskite matrix.

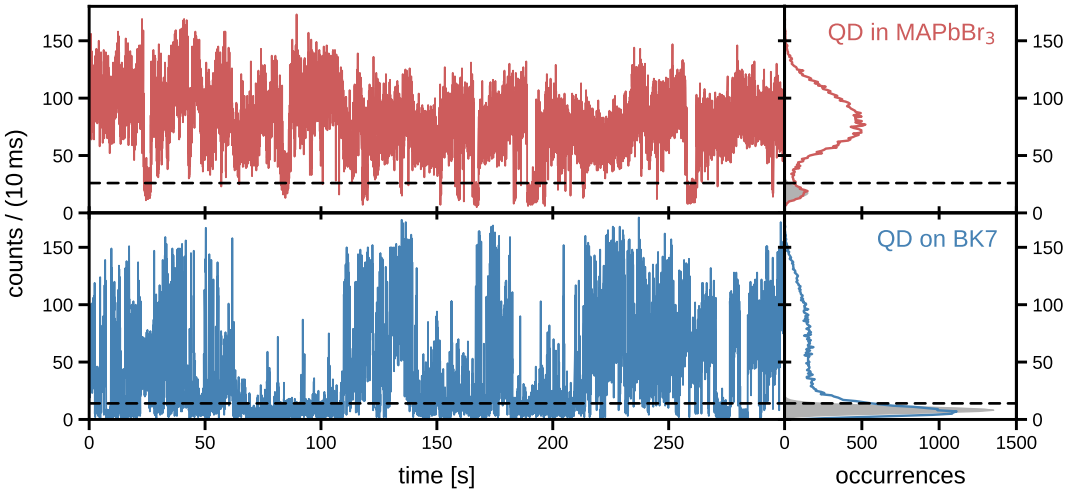

Figure S6: Comparison of the blinking behavior of a single QD-in-perovskite hybrid (top row, present work) and of an individual halide-capped QD on BK7 (bottom row, same data as in Fig. 5 c of Ref. S1). The main panels show PL intensity timetraces binned to 10 ms, while the side panels to the right present the corresponding count distributions, transposed to match the ordinates of the timetraces. The solid lines in the side panels are outlines of the count histograms and the gray areas indicate Poisson fits to the dim-state peaks, which served to establish the $p = 0.05$ threshold for probabilistic ON/OFF classification (dashed horizontal lines).

References

[S1] J. Baronnier, B. Mahler, O. Boisron, C. Dujardin, F. Kulzer and J. Houel, *Phys. Chem. Chem. Phys.*, 2021, **23**, 22750–22759.

[S2] V. LeBihan, A. Pillonnet, D. Amans, G. Ledoux, O. Marty and C. Dujardin, *Phys. Rev. B*, 2008, **78**, 113405.

[S3] A. Aubret, A. Pillonnet, J. Houel, C. Dujardin and F. Kulzer, *Nanoscale*, 2016, **8**, 2317–2325.

[S4] A. Aubret, V. Dolique, A. Piednoir, C. Dujardin, F. Kulzer and J. Houel, *Semicond. Sci. Technol.*, 2020, **35**, 055005.

[S5] D. E. Aspnes, *Am. J. Phys.*, 1982, **50**, 704–709.